

NON-LINEAR STRUCTURE FORMATION AND THE ACOUSTIC SCALE

HEE-JONG SEO^{1,2}, ETHAN R. SIEGEL², DANIEL J. EISENSTEIN², MARTIN WHITE^{3,4}

Accepted for publication in the Astrophysical Journal

ABSTRACT

We present high signal-to-noise measurements of the acoustic scale in the presence of nonlinear growth and redshift distortions using $320h^{-3}$ Gpc³ of cosmological PM simulations. Using simple fitting methods, we obtain robust measurements of the acoustic scale with scatter close to that predicted by the Fisher matrix. We detect and quantify the shift in the acoustic scale by analyzing the power spectrum: we detect at greater than 5σ a decrease in the acoustic scale in the real-space matter power spectrum of 0.2% at $z = 1.5$, growing to 0.45% at $z = 0.3$. In redshift space, the shifts are about 25% larger: we detect a decrease of 0.25% of at $z = 1.5$ and 0.54% at $z = 0.3$. Despite the nonzero amounts, these shifts are highly predictable numerically, and hence removable within the standard ruler analysis of clustering data. Moreover, we show that a simple density-field reconstruction method substantially reduces the scatter and nonlinear shifts of the acoustic scale measurements: the shifts are reduced to less than 0.1% at $z = 0.3 - 1.5$, even in the presence of non-negligible shot noise. Finally, we show that the ratio of the cosmological distance to the sound horizon that would be inferred from these fits is robust to variations in the parameterization of the fitting method and reasonable differences in the template cosmology.

Subject headings: distance scale — cosmological parameters — large-scale structure of universe — methods: N-body simulations — cosmology: theory

1. INTRODUCTION

Baryon acoustic oscillations (BAO) imprint a distinctive feature in the large-scale structure of both the cosmic microwave background and the matter density field. The sound waves propagating through the primeval plasma of photons and baryons in the early Universe freeze out when the photons are freed from baryons at the epoch of recombination. This leaves unique oscillatory features in the CMB (e.g., Miller et al. 1999; de Bernardis et al. 2000; Hanany et al. 2000; Lee et al. 2001; Halverson et al. 2002; Netterfield et al. 2002; Pearson et al. 2003; Benoît et al. 2003; Bennett et al. 2003; Hinshaw et al. 2007, 2008) as well as a lower contrast counterpart in the large-scale structure of matter (e.g., Peebles & Yu 1970; Sunyaev & Zeldovich 1970; Bond & Efstathiou 1984; Holtzman 1989; Hu & Sugiyama 1996; Hu & White 1996; Eisenstein & Hu 1998; Meiksin, White, & Peacock 1999; Eisenstein et al. 2005; Cole et al. 2005; Hütsi 2006; Tegmark et al. 2006; Percival et al. 2007a,b; Blake et al. 2007; Padmanabhan et al. 2007; Okumura et al. 2008; Estrada et al. 2008). The physical scale of the BAO is set by the distance that the sound waves have traveled before recombination, known as the sound horizon or acoustic scale. Since the sound horizon scale can be well determined by present and future CMB data, the BAO can serve as an excellent standard ruler (Hu & White 1996; Eisenstein et al. 1998; Eisenstein

2003; Blake & Glazebrook 2003; Hu & Haiman 2003; Seo & Eisenstein 2003). Observing the BAO from large-scale structure at different redshifts with the knowledge of their true physical scale allows us to geometrically measure the expansion history of the Universe and thereby identify the driving force behind the observed accelerated expansion, i.e., dark energy (e.g., Riess et al. 1998; Perlmutter et al. 1999).

Using the BAO as a standard ruler for precision cosmology requires that we understand all of the physical effects that could alter the acoustic scale during the evolution of the Universe. There are two important aspects of performance to consider for a standard ruler measurement with BAO: precision and accuracy. The precision of the standard ruler method crucially depends on the nonlinear evolution of structure growth and observational effects, such as redshift distortions and galaxy bias. With time, these nonlinear effects increasingly degrade the contrast of the BAO in the matter power spectrum and correlation function, decreasing the signal-to-noise of the standard ruler method. Recently, significant progress has been made on modeling the nonlinear evolution of the amplitude of the BAO with analytic and/or numerical methods (Meiksin, White, & Peacock 1999; Springel et al. 2005; Angulo et al. 2005; Seo & Eisenstein 2005; Angulo et al. 2005; White 2005; Jeong & Komatsu 2006; Crocce & Scoccimarro 2006; Eisenstein et al. 2007; Huff et al. 2007; Smith et al. 2007; Matarrese & Pietroni 2007; Smith et al. 2008; Angulo et al. 2008; Crocce & Scoccimarro 2008; Matsubara 2008; Takahashi et al. 2008; Sanchez et al. 2008) and on forecasting the resulting signal-to-noise for future galaxy redshift surveys (Blake & Glazebrook 2003; Linder 2003; Hu & Haiman 2003; Seo & Eisenstein 2003; Cooray 2004; Matsubara 2004; Amendola et al. 2005; Blake & Bridle 2005; Glazebrook & Blake 2005; Dolney et al. 2006; Zhan & Knox 2006; Blake et al.

¹ Center for Particle Astrophysics, Fermi National Accelerator Laboratory, P.O. Box 5 00, Batavia, IL 60510-5011; shee-jong@fnal.gov

² Steward Observatory, University of Arizona, 933 N. Cherry Ave., Tucson, AZ 85121

³ Departments of Physics and Astronomy, University of California, Berkeley, CA94720

⁴ Lawrence Berkeley National Laboratory, 1 Cyclotron Road, Berkeley, CA

2006; Seo & Eisenstein 2007). We can now make reasonable predictions for the degradation of the BAO due to nonlinear growth and redshift distortions.

The accuracy of the standard ruler method depends on the calibration of the physical scale of the BAO, i.e., the sound horizon. Future BAO surveys aim to push the standard ruler method to near the cosmic variance limit. This will require a calibration of the sound horizon scale to about 0.1% accuracy. However, nonlinear evolution not only degrades the precision of the standard ruler method by decreasing the contrast of the BAO, but also may alter [i.e., shift] the observed BAO scale in the large-scale structure at low redshift. Such a shift, relative to the linear acoustic scale derived from the CMB, will degrade the accuracy of the ruler. Failure to appropriately account for such a shift will result in biased measurements of the cosmological distances and therefore bias in the inferred dark energy parameters.

Previously, Seo & Eisenstein (2005) had no detection of a shift (or bias) in the acoustic scale at the $\sim 1\%$ level in the nonlinear real-space power spectrum from N-body data (also see Huff et al. 2007; Ma 2007; Eisenstein et al. 2007; Seo & Eisenstein 2007; Angulo et al. 2008; Sanchez et al. 2008). Meanwhile, Smith et al. (2008) predicts more than a percent level shift in the acoustic scale, when defining the observed scale as the local maxima of the peak in the correlation function (also see Smith et al. 2007; Guzik et al. 2007). However, the effect of the broadband shape, as well as the effect of the nonlinear smoothing of the BAO, on the shift of the acoustic scale can be largely marginalized over with appropriate parameterizations, which is probably the reason why such a large shift is not detected in Seo & Eisenstein (2005) and Angulo et al. (2008). That is, the choice of acoustic scale estimator matters; one cannot quantify a nonlinear shift without defining the estimator and one would surely prefer to use one that is close to optimal. The latter goal recommends template fitting to a significant portion of the power spectrum or correlation function, rather than peak finding methods.

Recent analytic and numerical work by Crocce & Scoccimarro (2008) makes use of renormalization perturbation theory and predicts a nonzero, irreducible shift at the few tenths of a percent level in real space due to nonlinear mode coupling. This is referred to as a “mode-coupling shift”; a similar context is introduced as “physical shifts” in Smith et al. (2008). The exact level of this mode-coupling shift would also depend on estimators: for example, the effects of the mode-coupling shifts that are different on different nodes may average out to some degree in the case of a global fit over several acoustic peaks. The good estimators will be ones that marginalize over most of the effects from the broadband shape and minimize contributions from the mode-coupling shifts. Any residual shifts can be modeled through numerical computation, such as a study of a large volume of N -body data.

In this paper, we show that most of the acoustic scale information can be extracted via a template fitting method. In order to test and confirm such a low level mode-coupling shift in redshift space as well as in real space, we require a very large volume of cosmological simulation. We use $320h^{-3} \text{ Gpc}^3$ of simulations to test the precision and the sub-percent level accuracy of

the standard ruler method with BAO. In this paper, we consider both nonlinear growth and redshift distortions. The effect of galaxy bias will be studied in our subsequent paper (Siegel et al., in preparation).

Eisenstein et al. (2007) show that a portion of the nonlinear degradation of the BAO can be undone with a simple reconstruction scheme based on the Zel’dovich approximation (also see Seo & Eisenstein 2007). We test how well we can undo the nonlinear shift as well as the erasure of the BAO, even given the presence of shot noise.

In § 2, we describe our cosmological N-body simulations and methods of χ^2 analysis to measure the acoustic scales from the simulations. In § 3, we present the resulting shifts and errors on the measurements of the acoustic scale when accounting for the nonlinear growth. In § 4, we proceed to redshift space, and present the effects of redshift distortions. In § 5, we show that not only the nonlinear erasure but also the nonlinear shift on the acoustic scale can largely be undone via reconstruction. In § 6, we compare our results of signal-to-noise with the Fisher matrix calculations. In § 7, we test how our results depend on the small errors on the template cosmology used in our fitting. Finally, in § 8, we summarize the major results obtained in this paper and point towards future directions for probing dark energy using BAO as a standard ruler.

2. SIMULATIONS AND THE METHODS OF ANALYSIS

We have chosen to investigate a specific cosmology of the Λ CDM family: $\Omega_m = 0.25$, $\Omega_\Lambda = 0.75$, $\Omega_b h^2 = 0.0224$, $h = 0.7$, $n = 0.97$ and $\sigma_8 = 0.8$. In order to model the non-linear evolution of structure, we make use of N-body simulations. Since our focus is on large scales and we need a lot of volume, we have elected to run 40 realizations of a $2h^{-1} \text{ Gpc}$ box using a parallel particle-mesh (PM) code. Each simulation employs 1024^3 particles on a 2048^3 force mesh, for a mesh resolution of $1h^{-1} \text{ Mpc}$ and a particle mass of $5 \times 10^{11} h^{-1} M_\odot$. The acoustic scale is thus resolved by ~ 100 grid cells in each dimension and the non-linear scale by ~ 10 cells. The initial conditions were generated using the Zel’dovich approximation (Zel’dovich 1970) starting from a regular grid at $z = 50$. The linear theory power spectrum for the initial conditions was computed by evolution of the coupled Einstein, fluid and Boltzmann equations using the code described in White & Scott (1996). Seljak et al. (2003) find that this code agrees well with CMBfast (Seljak & Zaldarriaga 1996). We used constant steps in $\ln a$ with steps of either 5% or 10%. The larger time steps resulted in a loss of power at small scales, but we saw no dependence on time step in the acoustic scale information.

Power spectra were computed at $z = 1.5, 1.0, 0.7$, and 0.3 by assigning the mass to a grid using the cloud-in-cell interpolation and using wavenumber bins of width $\Delta k = 0.0047 h \text{ Mpc}^{-1}$. In order to reduce the data volume that we need to store and manipulate, we save only 1% of the processed data for the later use (§ 5). In this paper, we use this 1% fraction only for our studies of reconstruction and shot noise.

We perform a χ^2 analysis to fit the spherically averaged power spectrum $P_{\text{obs}}(k)$ to template power spectra $P_m(k/\alpha)$. We parameterize the observed power spectra

as

$$P_{\text{obs}}(k) = B(k)P_m(k/\alpha) + A(k), \quad (1)$$

where α , $B(k)$, and $A(k)$ are fitting parameters. Here α is a scale dilation parameter and represents the ratio of the true (or linear) acoustic scale to the measured scale. For example, $\alpha > 1$ means that the measured BAO being shifted toward larger k relative to the linear power spectrum. In the case we fail to account for any nonlinear shift on the acoustic scale in the standard ruler method, α represents the ratio of the mis-measured distance to the true distance. The term $B(k)$ allows a scale-dependent nonlinear growth, and $A(k)$ represents an anomalous power, i.e., additive terms from the nonlinear growth and shot noise. By including both $B(k)$ and $A(k)$ with a large number of parameters, we minimize the contribution to the standard ruler method from the broadband shape of the power spectrum. We try various parameterizations for $B(k)$ and $A(k)$, as described in § 3 and § 4.

We calculate the model or template power spectrum P_m by modifying the BAO portion of the linear power spectrum with a nonlinear parameter Σ_m to account for the degradation of the BAO due to nonlinear effects and redshift distortions (Eisenstein et al. 2005; Tegmark et al. 2006; Crocce & Scoccimarro 2006; Eisenstein et al. 2007; Crocce & Scoccimarro 2008; Matsubara 2008):

$$P_m(k) = [P_{\text{lin}}(k) - P_{\text{smooth}}(k)] \exp[-k^2 \Sigma_m^2 / 2] + P_{\text{smooth}}(k), \quad (2)$$

where P_{lin} is the linear power spectrum and P_{smooth} is the nowiggle form from Eisenstein & Hu (1998). Any details of physics overlooked in the template power spectrum will be, at least partly, absorbed into $B(k)$ and $A(k)$. In fact, we will show that our results do not vary for a wide range of Σ_m , as the fitting formula can alter the amplitude of the BAO by trading power between $B(k)P_m$ and $A(k)$, as $B(k)$ and $A(k)$ have enough flexibility. Fine-tuning the choice of Σ_m in P_m does not affect our results, and therefore we do not include Σ_m as a fitting parameter. We use a fitting range of $0.02h \text{ Mpc}^{-1} \leq k \leq 0.35h \text{ Mpc}^{-1}$.

As the true covariance matrix of the N -body simulations is unknown a priori, we use the variation between the simulations to assess the true scatter in α . We fit each simulation assuming the covariance matrix for $P(k)$ is that of a Gaussian random field, i.e., assuming independent band powers with variances determined by the number of independent modes in each. While this is not an optimal weighting of the data for the determination of α , the effects from non-Gaussianity in the density field will still be reflected in the scatter between best-fit α 's from different simulations.

We use different groupings to assess the scatter between our simulations. Our primary approach is to measure the scatter in α from jackknife sampling of the 40 simulations. However, we have also used bootstrap sampling for 40 sets of 1 simulation. The results from the two approaches are highly consistent; we will quote results for the jackknife case. Note that the scatter in α , i.e., σ_α , that we quote represents the scatter associated with the mean value of α for a total volume of $320h^{-3} \text{ Gpc}^3$, not the scatter between samples.

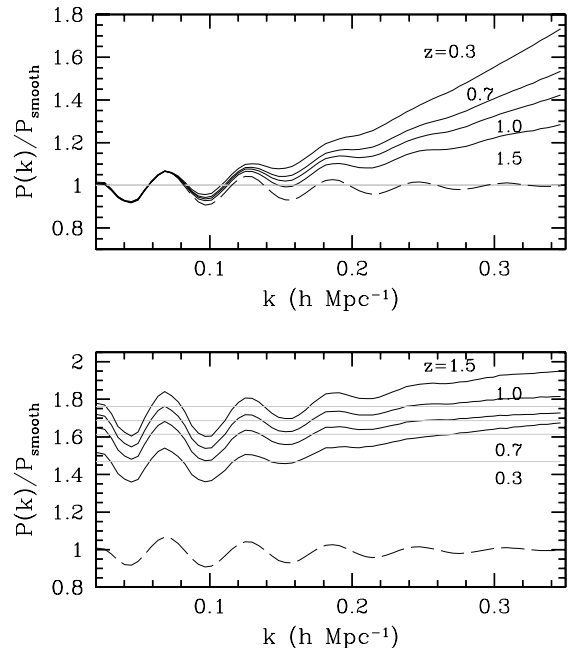


FIG. 1.— Real-space (top) and redshift-space (bottom) power spectrum $P(k)$ from our N -body simulations for $z=0.3, 0.7, 1.0,$ and 1.5 . The power spectra are divided by P_{smooth} , the nowiggle form from Eisenstein & Hu (1998), scaled with D^2 . The dashed line is the linear power spectrum. The gray lines indicate the large-scale amplitude expected from linear theory.

3. A REAL-SPACE ANALYSIS OF THE BAO

3.1. Non-linear Growth of Structure

Nonlinear growth arises when the density perturbation on a given scale reaches an amplitude of order unity; the evolution of perturbations of different wave modes becomes increasingly coupled with one another, causing a substantial departure from linear evolution (e.g., Juszkiewicz 1981; Vishniac 1983; Makino et al. 1992; Jain & Bertschinger 1994; Bharadwaj 1996a,b; Meiksin & White 1999; Scoccimarro et al. 1999). Such a nonlinear process erases the BAO of the power spectrum (e.g., Meiksin, White, & Peacock 1999; Seo & Eisenstein 2005), thereby degrading the signal of the standard ruler method. It also increases small-scale power above the linear growth rate, thereby increasing the noise in the clustering statistics. This nonlinear process first appears on small scales and proceeds to larger scales with time. From the perspective of configuration space, the nonlinear growth damps the BAO peak at $\sim 100h^{-1} \text{ Mpc}$ because the large-scale bulk flows cause the differential motions of the density pairs initially separated by the sound horizon scale (Eisenstein et al. 2007). In this section, we measure the effect of nonlinear structure growth on the BAO using the real-space power spectra from our N -body simulations.

3.2. Fitting Results in Real Space

In the upper panel of Figure 1, we illustrate the spherically-averaged real-space power spectra from our N -body simulations for each of our four redshifts (0.3, 0.7, 1.0, and 1.5), divided by the nowiggle form from Eisenstein & Hu (1998). As expected, the effect of non-linearity increases the small-scale power and increasingly degrades the BAO at lower redshifts.

We measure the shifts and the scatters of the shifts of the BAO relative to linear theory with a χ^2 analysis. We model the real-space nonlinear power spectrum by parameterizing $B(k)$ and $A(k)$ in equation (1) in two independent ways. We use polynomial fitting, which we refer to as “Poly7”, with

$$\begin{aligned} \text{“Poly7”}: B(k) &= b_0 + b_1k + b_2k^2, \\ A(k) &= a_0 + a_1k + a_2k^2 + \dots + a_7k^7, \end{aligned} \quad (3)$$

as well as fitting to Pade approximants, which we refer to as “Pade”, where

$$\begin{aligned} \text{“Pade”}: B(k) &= b_0 \frac{1 + c_1k + c_3k^2 + c_5k^3}{1 + c_2k + c_4k^2}, \\ A(k) &= a_0 + a_1k + a_2k^2. \end{aligned} \quad (4)$$

Here a_i , b_i , and c_i are free fitting parameters for all i . In addition, we consider a case in which $A(k)$ in equation (3) is truncated at third order in k , which we refer to as “Poly3”. In constructing P_m , we use reasonable choices of Σ_m that are based on the Zel’dovich approximations (Eisenstein et al. 2007): $7.6h^{-1}$ Mpc at $z = 0.3$ and scaling with the linear growth factor at other redshifts. We vary Σ_m near our fiducial values so as to show that the analysis is not sensitive to the choice of Σ_m .

We perform a jackknife analysis on our 40 simulations of $P(k)$, using the two different fitting forms above. We detect non-zero shifts on the mean acoustic scale [i.e., $\alpha - 1$] of a few tenths of a percent at all redshifts, as shown in Table 1. These shifts represent a decrease in the fitted acoustic scale [i.e., the fitted BAO being at larger k], as opposed to the linear scale, of 0.20%, 0.26%, 0.33%, and 0.45% for respective redshifts of 1.5, 1.0, 0.7, and 0.3. The shifts increase at lower redshifts, as expected from the evolution of nonlinear structure. Our results are statistically significant at the 5σ , 6σ , 7σ , and 8σ levels for respective redshifts of 1.5, 1.0, 0.7, and 0.3, for both fitting forms. The reduced χ^2 values in the table are obtained from the best fit to the averaged power spectrum over 40 simulations and show the goodness of the fit in general. The reduced χ^2 , χ^2/DOF , is close to unity even though we have used a Gaussian approximation for the errors on the nonlinear power spectrum.

Our results are consistent over a wide range of Σ_m ($\Delta\Sigma_m = \pm 2h^{-1}$ Mpc) used in P_m , as shown in the lower half of Table 1: the difference in α is well within σ_α and the difference in σ_α is well within the expected Gaussian sample variance of $1/\sqrt{2} \times 40 \approx 11\%$ for 40 simulations. For example, varying Σ_m between $6.0h^{-1}$ Mpc and $9.0h^{-1}$ Mpc at $z = 0.3$ causes negligible changes in α and σ_α (less than 10^{-4} in α). Reasonable variations at other redshifts are similarly negligible. That is, due to the large number of parameters allowed in our parameterization, our fitting is able to tolerate a mild discrepancy between Σ_m used in P_m and the actual power spectrum, without a substantial degradation of the fit.

While the “Pade” model gives a slightly better fit than the “Poly7” model, based on the smaller χ^2/DOF values, we note that both models give the same acoustic peak scale and very similar errors. We tried varying the order of the fitting formulae and found that our results did not change. Of course, one cannot make $B(k)$ and $A(k)$ arbitrarily flexible or else these terms would be able to mimic the BAO. With a fitting range

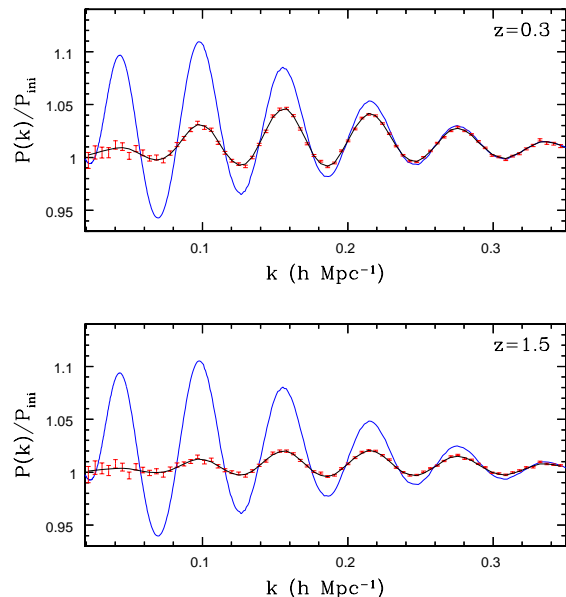


FIG. 2.— Real-space power spectra at $z = 0.3$ and 1.5 divided by the initial linear power spectrum: we divide $P_{\text{res}} = (P_{\text{nl}} - A(k))/B(k)$ by P_{lin} . The oscillatory feature represents the amount of degradation of the BAO. Red error bars are Gaussian errors centered at $P_{\text{res}}/P_{\text{lin}}$. Black solid lines are for the template power spectra $P_m(k/\alpha)/P_{\text{lin}}(k)$ constructed by using $\Sigma_m = 7.6h^{-1}$ Mpc and $4.5h^{-1}$ Mpc at $z = 0.3$ and 1.5 , respectively. Blue solid lines represent the nowiggle form, i.e., $P_{\text{smooth}}(k/\alpha)/P_{\text{lin}}(k)$.

of $0.02h \text{ Mpc}^{-1} \leq k \leq 0.35h \text{ Mpc}^{-1}$, the flexibility we allowed in both our fitting formula avoids this problem. As shown in Table 1, decreasing the polynomial orders of $A(k)$ to the third order, i.e., “Poly3”, makes a negligible change to the best-fit α and σ_α . However, using a model in which $B(k)$ is constant produced notably worse fits and made the fit more sensitive to the choice of Σ_m used in P_m . To be conservative, we recommend a second order $B(k)$ and higher than fourth order in $A(k)$ in real space.

We find that the bootstrap analysis is highly consistent with the jackknife estimate of the scatter in α . Both agree to within 5% in σ_α and 0.0001 in α .

Figure 2 shows the real-space average power spectrum at $z = 1.5$ and 0.3 , and, as a comparison, the best-fit models to them. Here, we first subtract the additive part $A(k)$ from the nonlinear power spectra and then divide the residual $P_{\text{nl}} - A(k)$ by $B(k)$ and by the input linear power spectrum, so as to manifest the degradation in the BAO feature. That is, the broad-band differences, relative to the initial power spectrum, have been removed and only the difference in the BAO structure is illustrated: any oscillations in the figure represents the nonlinear *erasure* of the BAO. We note that the BAO feature in Figure 2 depends on the value of Σ_m we assume for the template P_m . The results at $z = 0.7$ and 1 are similar to the redshifts shown. Error bars are drawn assuming Gaussian errors, which will be an underestimation on small scales, where there should be a contribution from the trispectrum. We also ignore the nonlinear covariance between the different data points in the figure. The excellent agreement between the best-fit power spectrum and the N -body data demonstrates that our template model has a suitable amount of flexibility to match the data well.

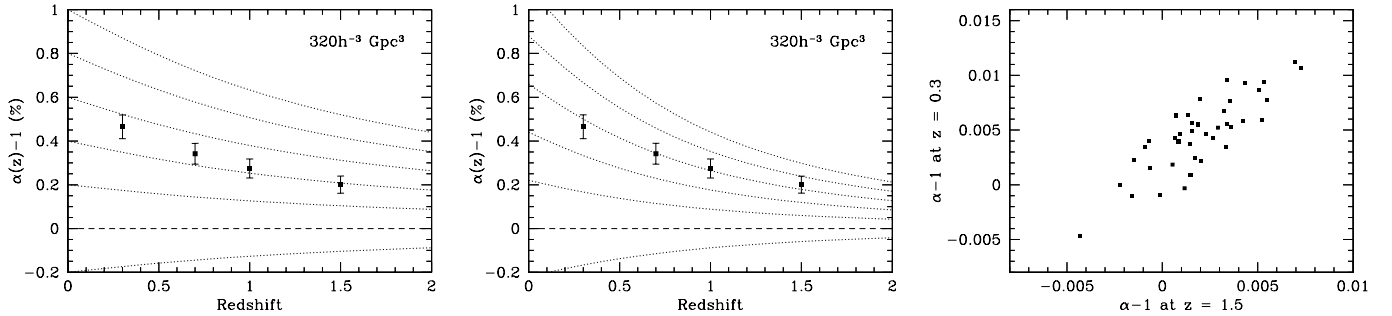


FIG. 3.— Left and Middle panels: the growth of nonlinear shift in $\alpha - 1$ with redshift. The data points show the mean of α as a function of redshift; the errors show the scatter. The points are correlated. In the left panel, we overplot curves proportional to D^1 ; in the middle panel, we overplot curves proportional to D^2 . Right panel: the $\alpha - 1$ at $z = 0.3$ and $z = 1.5$ for 40 simulations. One can see that a given simulation produces α that are highly correlated between redshifts.

To conclude, we find shifts of 0.2% to 0.45% in the acoustic scale due to nonlinear growth. The shifts increase at lower redshifts. Our recovery of the acoustic scale from the template fitting method is robust for different fitting forms, a wide range of Σ_m , and the choice of jackknife or bootstrap resampling.

3.3. The Growth of $\alpha - 1$ with Redshift

We next investigate the redshift dependence of the shift α . The left and the middle panel of Figure 3 shows the growth of $\alpha - 1$ with redshift with the error bars σ_α for $320h^{-3} \text{ Gpc}^3$. The dotted lines are curves of linear growth with different proportionality constants in the left panel, and are curves scaling quadratically with the growth factor in the middle panel. From the figure, $\alpha - 1$ is growing faster than the growth factor, D , but slower than D^2 . We find that $\alpha - 1$ scales as D^m where $m = 1.66^{+0.26}_{-0.22}$, when we perform a χ^2 fitting to the mean α with a covariance matrix generated by the variations in the bootstrap samples. The right panel shows that values of $\alpha - 1$ for each subsample are highly correlated between different redshifts, as expected. A model of $\alpha - 1$ scaling as D^2 , which one might expect from the perturbation theory (Croce & Scoccimarro 2008), is only 1.3σ away from the best fit; we cannot reject this model. Meanwhile, $\alpha - 1$ scaling as D is disfavored at about 3σ . However, a model with leading order D and higher-order terms fits well and cannot be excluded.

We next compare our results with the analytic predictions. While we detect the sub-percent level nonlinear mode-coupling shift predicted by Smith et al. (2008) and Croce & Scoccimarro (2008) (also see Nishimichi et al. 2007), the redshift-dependence of $\alpha - 1$ we derive is weaker than the node-by-node shifts in the BAO feature in power spectrum predicted by Croce & Scoccimarro (2008), where they simulate the fitting method used in Percival et al. (2007b)⁵. Note, however, that we are using a global fit, where the overall shift will be a result of different nodes being weighed differently depending on redshift, resulting in an overall redshift dependence that is not the same as the redshift dependence of individual nodes. Indeed, when they consider a global fit, the redshift dependence of the shift seems attenuated [Eq. (27) of Croce & Scoccimarro (2008)]. In addition, other details of our fitting method are different from the cases

⁵ Their α corresponds to the inverse of α defined in this paper.

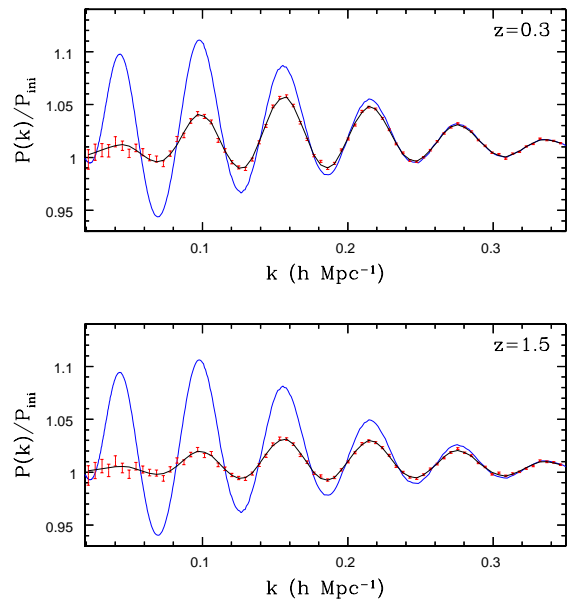


FIG. 4.— Redshift-space power spectra at $z = 0.3$ and 1.5 divided by the initial linear power spectrum: we divide $P_{\text{res}} = (P_{\text{nl}} - A(k))/[B(k)F_{\text{fog}}]$ by P_{lin} . The oscillatory feature represents the amount of degradation of the BAO. Red error bars are Gaussian errors centered at $P_{\text{res}}/P_{\text{lin}}$. Black solid lines: $P_m(k/\alpha)/P_{\text{lin}}(k)$ constructed by using $\Sigma_m = 9.0h^{-1} \text{ Mpc}$ and $6.0h^{-1} \text{ Mpc}$ at $z = 0.3$ and 1.5 , respectively. Blue solid lines represent the nowiggle form, i.e., $P_{\text{smooth}}(k/\alpha)/P_{\text{lin}}(k)$.

they considered. Taking these differences into account, we consider that these analytic works and our N -body results are largely in agreement.

4. A REDSHIFT-SPACE ANALYSIS OF THE BAO

4.1. Redshift-space Distortions

The observed power spectrum is subject to redshift-space distortions due to the peculiar velocity of the observed sources. The large-scale bulk motions [i.e., outflow from underdense regions and infall toward overdense regions] along the line of sight increase the apparent density contrast in this direction and induce an angle-dependent amplification of the real-space power spectrum on large scales (Kaiser 1987; Hamilton 1998; Scoccimarro 2004; Papai & Szapudi 2008, etc). The apparent displacements due to such redshift distortions degrade the BAO further in redshift space relative to real space (e.g., Meiksin, White, & Peacock 1999; Seo & Eisenstein 2005;

Eisenstein et al. 2007). Meanwhile, virial motions between and within halos cause an apparent suppression of the small-scale power along the line of sight, which is called the finger-of-God effect (FoG) (de Lapparent et al. 1986).

While the redshift distortions are an inevitable element of the study of cosmological distance error estimation, a direct χ^2 analysis of the redshift-space power spectrum has been challenging due to the lack of a reliable model for fitting redshift distortions and the anisotropic nature of the redshift-space power spectrum (cf., Wagner et al. 2007; Angulo et al. 2008; Okumura et al. 2008; Padmanabhan & White 2008). Recent theoretical and numerical studies (Eisenstein et al. 2007; Matsubara 2008), however, provide quantitative predictions for the BAO degradation due to nonlinearity and redshift distortions and therefore for the resulting distance errors (e.g., Seo & Eisenstein 2007). Based on these studies, we can improve the description of the nonlinear effect on BAO in the fitting model and check the distance errors derived from the redshift-space power spectra.

In this section, we extend the χ^2 analysis to the spherically-averaged redshift-space power spectrum to find the effect of the redshift distortions on the acoustic scale measurements. We do not include large-angle effects in the redshift distortions but merely use the flat-sky approximation. Due to a computer hardware problem, some of the redshift-space data were lost, so that our redshift-space analysis uses a volume of $216h^{-3}$ Gpc³ (i.e., 27 simulations).

4.2. Fitting Formulae

The lower panel of Figure 1 shows the spherically averaged redshift-space power spectra from our simulations. In order to account for the FoG effect in a χ^2 analysis, we add a simple multiplicative function F_{fog} to our parameterization. We try two ways of incorporating F_{fog} into our parameterization:

$$\text{“In”}: P(k) = B(k)P_m(k/\alpha)F_{\text{fog}} + A(k), \quad (5)$$

and

$$\text{“Out”}: P(k) = [B(k)P_m(k/\alpha) + A(k)] \times F_{\text{fog}} + e_1. \quad (6)$$

where $A(k) = a_0 + a_1k + a_2k^2$. Note that the highest order of polynomials for $A(k)$ is only k^2 , less than that of “Poly7” in real space. We lower the number of parameters in $A(k)$ in redshift space, as there are enough additional parameters to account for the broad-band shape. The parameter e_1 is added to permit a shot noise term in the “Out” model.

We again try both polynomial and Pade approximants for $B(k)$:

$$\text{“Poly”}: B(k) = b_0 + b_1k + b_2k^2 \quad (7)$$

and

$$\text{“Pade”}: B(k) = b_0 \frac{1 + c_1k + c_3k^2 + c_5k^3}{1 + c_2k + c_4k^2}. \quad (8)$$

We try two forms for F_{fog} :

$$\text{“Rat”}: F_{\text{fog}} = 1 / [1 + (kd_1)^{d_2}]^{1/d_2} \quad (9)$$

with priors of $d_1 > 0.1h^{-1}$ Mpc and $d_2 > 0$, and

$$\text{“Exp”}: F_{\text{fog}} = \exp[-(kd_1)^{d_2}] \quad (10)$$

with priors of $d_1 > 0h^{-1}$ Mpc and $d_2 > 0$. We refer to, for example, the combination of equations (7) and (10) in the form of equation (6) as “Poly-Exp-Out”. In addition, we also try “Poly7” (eq. [3]) to fit the redshift-space power spectrum. We will mainly quote the results from using “Poly-Exp-Out”.

We increase the values of Σ_m used in P_m relative to the choices in real space, so as to account for the additional degradation of the BAO due to redshift distortions. Note that we are approximating the anisotropic nonlinear effect on the BAO in redshift space with an isotropic parameter Σ_m .

4.3. Fitting Results in Redshift Space

Table 2 lists the errors and the mean of the best-fit α of jackknife samples in redshift space. We also present the values of σ_α rescaled to a survey volume of $320h^{-3}$ Gpc³ from the actual results for $216h^{-3}$ Gpc³ so as to provide an easy comparison to Table 1.

We again detect a non-zero, sub-percent shift of the mean values of α in redshift space: 0.25% of shift of the acoustic scale at $z = 1.5$ by 5σ , 0.33% at $z = 1$ by 5σ , 0.41% at $z = 0.7$ by 6σ , and 0.54% at $z = 0.3$ by 6σ , where the signal-to-noise ratios are calculated based on the original σ_α for $216h^{-3}$ Gpc³. The shift on α has systematically increased relative to the real-space values at all redshifts. We find that α increases by $\sim 25\%$ at all redshifts; we do not detect a redshift-dependence in this increase. As expected, values of σ_α also have increased relative to the real-space values at all redshifts: about 25% at $z = 0.3$ and 0.7 , 18% at $z = 1$, and 11% at $z = 1.5$.

We find our results to be consistent for both α and σ_α , regardless of the various parameterizations. As shown in Table 2 for $z = 0.3$, the differences in α are well within σ_α and the differences in σ_α are well within the sample variance, $1/\sqrt{2 \times 27} \approx 14\%$, in most of the cases. Interestingly, we find that even without correcting for F_{fog} , such as the real-space fitting formula “Poly7” (eq [3]), yields results consistent with ones with F_{fog} correction, so long as enough free fitting parameters are allowed. Again, the results are not very sensitive to the fiducial values of Σ_m used to calculate P_m . We therefore choose equation (6) combined with the polynomial $B(k)$ and the exponential form of F_{fog} (i.e., eq [10]), “Poly-Exp-Out”, as our convention to fit the redshift-space power spectra for the rest of paper.

Figure 4 shows the redshift-space power spectrum at $z = 1.5$ and 0.3 and the best-fit models to them. Again, we first subtract the additive part $A(k)$ from the nonlinear power spectra, but this time we divide the residual $P_{\text{nl}} - A(k)$ by $B(k)F_{\text{fog}}$ before dividing by the input linear power spectrum, so as to manifest the degradation in the BAO feature. The figure illustrates the excellent agreement between the best-fit power spectrum and the N -body data.

5. RECONSTRUCTING THE BAO

In this section, we reconstruct the baryon acoustic signature obscured by nonlinear growth and redshift distortions using the simple scheme presented in

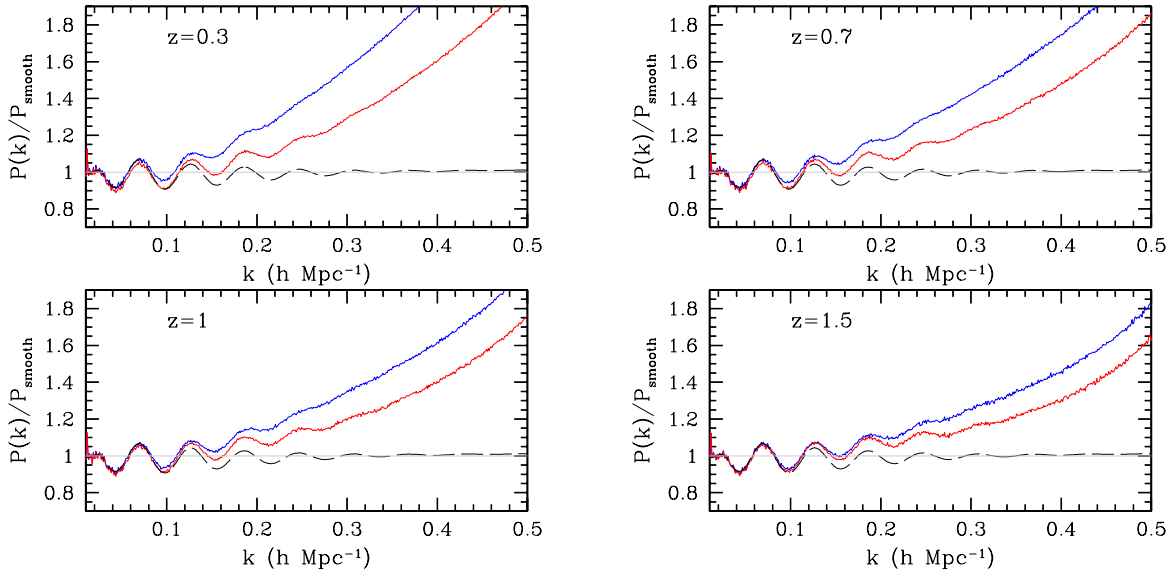


FIG. 5.— Real-space $P_{\text{nl}}(k)$ of the 1%-sample after reconstruction (red lines), divided by the nowiggle form from Eisenstein & Hu (1998), in comparison to the nonlinear power spectra before reconstruction (blue lines). The gray lines are for the large-scale amplitude expected from linear theory. The dashed lines are for linear power spectrum. The effect of reconstruction is most apparent at $z = 0.3$ and is smallest at $z = 1.5$.

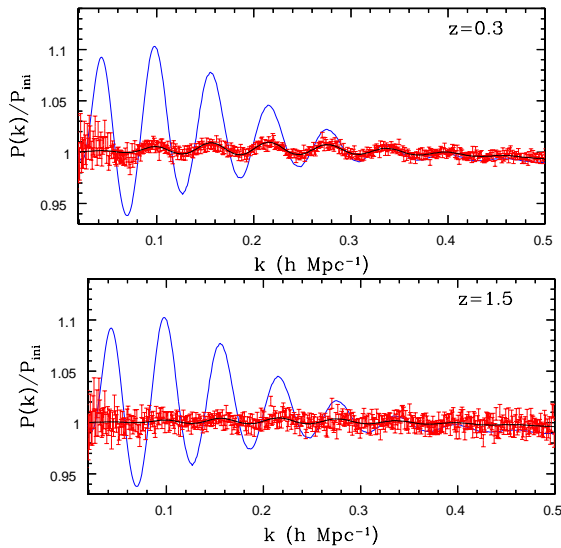


FIG. 6.— Real-space $P_{\text{nl}}(k)$ of the 1%-sample after reconstruction (red error bars): we divide $P_{\text{res}} = (P_{\text{nl}} - A(k))/B(k)$ by P_{lin} . The oscillatory feature represents the amount of degradation of the BAO. Red error bars are Gaussian errors centered at $P_{\text{res}}/P_{\text{lin}}$. Black solid lines are for the template power spectra $P_m(k/\alpha)/P_{\text{lin}}(k)$ constructed by using Σ_m listed in Table 3. Blue solid lines: $P_{\text{smooth}}(k/\alpha)/P_{\text{lin}}(k)$.

Eisenstein et al. (2007). We wish to investigate whether such reconstruction improves the signal-to-noise ratio on the measurement of α (Seo & Eisenstein 2007) and whether it reduces the shift of the acoustic scale.

For the analysis with reconstruction, we use the phase-space data of a randomly selected 1% of all the particles. We will refer to this sample as “1%-sample”, in comparison to the previous “100%” sample. For the 1% sample, power spectra are computed for wavenumber bins of width $\Delta k = 0.001 h \text{ Mpc}^{-1}$ and we use a fitting range of $0.02 h \text{ Mpc}^{-1} \leq k \leq 0.5 h \text{ Mpc}^{-1}$. We utilize a volume of $320 h^{-3} \text{ Gpc}^3$ both in real space and in redshift space. We note that by using the 1% sample, we perform the reconstruction scheme in the presence of non-negligible

shot noise. Seo & Eisenstein (2007) quantify the ratio of shot noise to sample variance with $nP_{0.2}$, where n is the number density and $P_{0.2}$ is the real-space power at $k = 0.2 h \text{ Mpc}^{-1}$. For the analysis here, $nP_{0.2}$ runs from 0.7 at $z = 1.5$ to 2.4 at $z = 0.3$.

We apply the linear perturbation theory continuity equation to the nonlinear density fields of the 1%-sample and predict the linear theory motions. We first take the nonlinear density fields at $z=0.3, 0.7, 1.0,$ and 1.5 and Fourier-transform them. We apply a $10 h^{-1} \text{ Mpc}$ Gaussian filter to $\delta(k)$ in order to smooth gravity on small scales. We then compute the linear theory motions \vec{q} using $\nabla \cdot \vec{q} = -\delta$. Finally we displace the real particles and smoothly distributed reference particles by the resulting \vec{q} , and find the final density field from the difference of the two density fields. As Eisenstein et al. (2007) noted, this differencing method moves the measured *densities* back to their initial locations: linear structure growth is mostly preserved and only the nonlinear growth effect is reduced as a result.

5.1. Reconstruction in Real Space

Figure 5 shows the reconstructed power spectra of the 1% sample, divided by P_{smooth} , at various redshifts. The benefits of reconstruction are most obvious at $z = 0.3$ due to the low shot noise and the strong nonlinearity to correct for at this redshift. We fit the power spectra of these reconstructed density fields using the same models as before (eq. [3] and [4]). We find consistent results for both models in general. Because the upper limit of the fitting range was chosen to be $k = 0.5 h \text{ Mpc}^{-1}$ in the 1% case, we find that the “Poly7” model with more flexible $A(k)$ fits better to the reconstructed real-space power. We decrease Σ_m for the template P_m approximately by half relative to Σ_m values used before reconstruction.

Table 3 shows the resulting $\alpha - 1$ and σ_α for the “Poly7” model. Because the reconstruction analysis uses the 1% sample, the results in Table 3 are not immediately comparable to those in Table 1, which used the 100% sample

and hence had negligible shot noise. We include results for the 1% sample without reconstruction in Table 3 to provide the proper comparison.

We find that applying reconstruction decreases σ_α by almost a factor of 2 at $z = 0.3$. The improvement is incrementally less at higher redshifts. This is to be expected for several reasons. First, the density field is more linear at high redshift. As most of the acoustic scale information is at $k \lesssim 0.2h \text{ Mpc}^{-1}$, the non-linear degradation of σ_α is smaller at high redshift. There is therefore less for the reconstruction algorithm to fix. Second, the intrinsic clustering is weaker at high redshift such that the shot noise is more important. This contaminates the measurement of the density field and hence the estimation of the reconstruction displacements, causing the reconstruction to be less accurate. Third, the increased shot noise means that the high harmonics are not being well measured, regardless of whether or not they are correctly reconstructed. This means that the results with and without reconstruction will not differ much. For example, the comparison of Tables 1 and 3 (summarized in the ‘‘N-body’’ column of Table 5) shows that the introduction of shot noise degrades σ_α by over a factor of 2 at $z = 1.5$, even without reconstruction. Finally, the force resolution of our PM simulations ($1h^{-1} \text{ Mpc}$ mesh) may not be adequate to recover the BAO with full fidelity when our reconstructed Σ_m is expected to be as small as $2 - 3h^{-1} \text{ Mpc}$, as it is at $z > 1$. If our small-scale structure is more fluffy, this will appear as an extra source of Σ_m .

In addition to the improvement in the scatter of α , Table 3 also shows that reconstruction decreases the shifts in α itself. The shift in α decreases to 0.07% at $z = 0.3$ and to below 0.03% at higher redshifts. Note that while reconstruction does not improve σ_α at $z = 1.5$, it does substantially improve the shift in α . This likely indicates that the reconstruction method is correctly compensating for the large-scale bulk flows but is leaving a small-scale jitter that washes out the high harmonics of the BAO, as discussed above. Figure 6 shows the best-fit models to the averaged power spectra of the 1%-sample after reconstruction. Increasing the Gaussian filter size to $14h^{-1} \text{ Mpc}$ makes no difference: less than 2% in σ_α and 10^{-4} in α .

5.2. Reconstruction in Redshift Space

Next we apply the reconstruction techniques to the redshift-space density field. The method is unchanged, save that we use the observed nonlinear redshift-space density field and apply the resulting displacement field to the redshift-space positions (Eisenstein et al. 2007). In this paper, we do not attempt to correct for the FoG effect of virialized halos (c.f., Eisenstein et al. 2007).

Figure 7 shows the redshift-space power spectra after reconstruction, divided by the nowiggle form; the difference before and after reconstruction is significant even in redshift space, not only at $z = 0.3$ but also at $z = 0.7$ and 1.0. Table 4 quantifies the values of α and its scatter after applying the reconstruction method in redshift space. We find that the scatter σ_α is substantially reduced to a level comparable to that found with the reconstructed real-space case. That is, the reconstruction method seems more effective in redshift space. The BAO is more smeared in redshift space, providing more oppor-

tunity for reconstruction to improve σ_α . In addition, the higher amplitude of the power spectra in redshift space reduces the effects of shot noise and may permit better reconstruction.

As in real space, the shifts in the acoustic scale, α , are markedly improved, decreasing to below 0.1% at all redshifts. Figure 8 shows the resulting best-fit to the averaged power spectra, compared to the data. Again, we find a good agreement between the two.

6. COMPARING THE N-BODY RESULTS TO THE FISHER MATRIX PREDICTION

We next compare σ_α from the N -body data with the analytic distance error estimates from the Fisher matrix formalism. We calculate the Fisher matrix estimates by using a fitting formula based on Seo & Eisenstein (2007). This formula uses a parameter Σ_{nl} to quantify the amount of non-linear degradation of the BAO. We estimate a reasonable value of Σ_{nl} at each redshift by using the analytic Zel’dovich approximations (eq. [9] of Eisenstein et al. (2007)).

Table 5 compares σ_α from the N -body data with the Fisher matrix estimates. We start with the Fisher matrix errors corresponding to the 100% samples, for which shot noise is negligible; we use $nP_{0.2} = 100$ for all redshifts. We do not include the nonlinear growth effect into $nP_{0.2}$, following the convention in Seo & Eisenstein (2007). While the Fisher matrix errors are in reasonable agreement with the N -body data, the Fisher matrix calculation systematically overestimates σ_α by $\sim 25\%$, 17%, 15%, and 5% at $z = 0.3, 0.7, 1.0,$ and 1.5, respectively, as shown in Table 5. Such an overestimation is contrary to our intuition that the N -body data would reflect extra nonlinear effects, such as an effect on variance of the power spectrum, that the Fisher matrix does not incorporate. As we allow many free parameters in our fitting forms, the contribution to the standard ruler method from the broad-band shape of the power spectrum is negligible. However, because σ_α is estimated from only 40 simulations, the error on the scatter is expected to be $1/\sqrt{2 \times 40} \approx 11\%$, assuming Gaussianity. While the discrepancy becomes larger than the expected sample variance at $z \leq 1$, it is possible that the N -body results are lower than the Fisher matrix predictions simply because of sample variance. Because α values in a simulation are largely correlated between redshifts, it would not be surprising that the residuals in σ_α could all have the same sign.

For the 1%-samples (Table 5), shot noise is not negligible. We derive $nP_{0.2}$ from the nominal shot noise, i.e., the inverse of the number density of particles. We find that the Fisher matrix errors are bigger than those from the simulations by 18% and 23% at $z = 0.3$ and 0.7, respectively. At $z = 1.0$ and 1.5, the agreement is better. The degradation in σ_α from the simulation due to the addition of shot noise appears well predicted by the Fisher matrix formula. We note that the shot noise and its effect on α is not correlated between redshifts, leading to a little more scatter around the redshift trends.

We next compare σ_α from the N -body data with the Fisher matrix errors in redshift space. We use the 2-dimensional [2-D] approximation based on Seo & Eisenstein (2007) and contract the 2-D matrix to derive the 1-D distance error, as the transverse and the

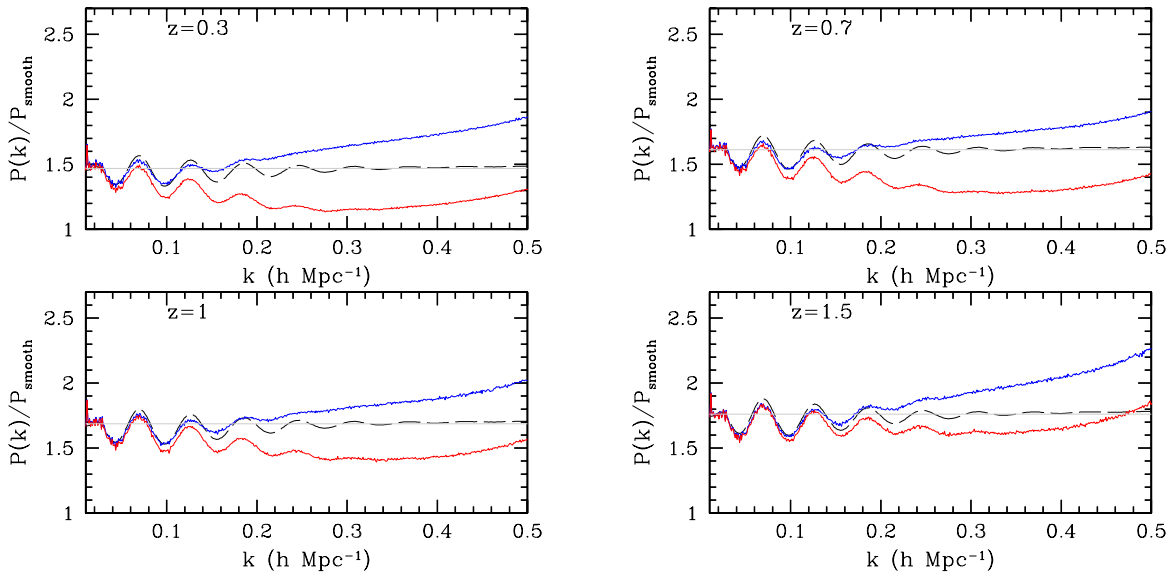


FIG. 7.— Redshift-space $P(k)$ of the 1%-sample after reconstruction (red lines), divided by the nowiggle form, in comparison to the redshift-space nonlinear power spectra before reconstruction (blue lines). The gray lines are for the large-scale amplitude expected from linear theory. The dashed lines are for linear power spectrum. The effect of reconstruction is most apparent at $z = 0.3$ and is smallest at $z = 1.5$.

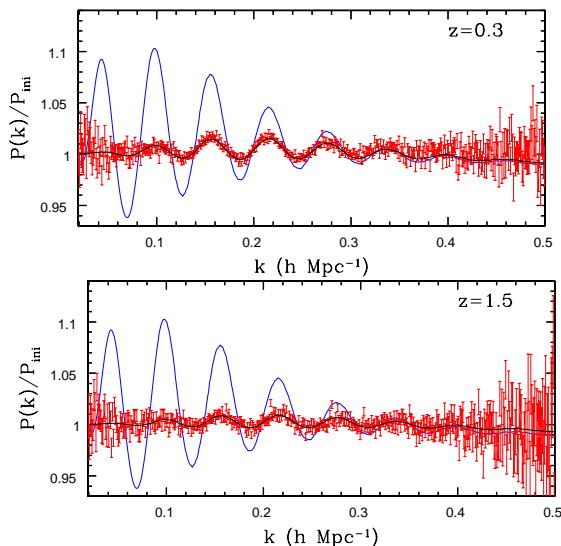


FIG. 8.— Redshift-space power spectra of the 1%-sample after reconstruction (red error bars), in comparison to the best-fit models (black lines) and nowiggle form (blue lines): we divide $P_{\text{res}} = (P_{\text{nl}} - A(k))/B(k)/F_{\text{fog}}$ by P_{lin} .

line-of-sight distance scales are the same in this simulated Universe. We use an ellipsoidal smoothing kernel with $\Sigma_{\text{xy}} (= \Sigma_{\text{nl}})$ and $\Sigma_z = [1 + \Omega_m(z)]^{0.6} \Sigma_{\text{xy}}$ and include the angle dependence in $nP_{0.2}$. The FoG effect is not included in $nP_{0.2}$, as justified in Seo & Eisenstein (2007).

From Table 5, the σ_α values from the 100%-samples deviate from the Fisher matrix errors approximately by 1.5 times the sample variance. Again, they are systematically lower than the Fisher matrix errors. Note that we expect the sample variance of $1/\sqrt{2} \times 27 \approx 14\%$ rather than $1/\sqrt{2} \times 40$ in this case. For the 1%-samples, the discrepancy reaches up to 27% at $z = 0.3$, while the discrepancy is below the sample variance of $1/\sqrt{2} \times 40 \approx 11\%$ at high redshift.

Overall we find that the distance errors from the

N -body data in real and redshift space are somewhat smaller than the Fisher matrix errors with Σ_{nl} based on the Zel'dovich approximations. The measured errors from the N -body data correspond to reductions of Σ_{nl} by as much as $1h^{-1}$ Mpc relative to the Zel'dovich prediction. It is possible that this systematic discrepancy is merely due to sample variance, which is expected to be correlated between redshifts. However, there could be other reasons for the difference. It is possible that the Zel'dovich approximation slightly overestimates the non-linear degradation (Crocco & Scoccimarro 2006, Padmanabhan & White, in preparation) or that the approximations behind the Fisher matrix calculation are slightly pessimistic. Previous comparisons to high-resolution N -body simulations (Seo & Eisenstein 2007) found agreement to better than 13%, comparable to the precision tested here. In principle, we could try to use the amplitude of the wiggles in $P(k)$ to estimate Σ_{nl} , but our template fitting parameter Σ_m is not a precise proxy for Σ_{nl} because the marginalization parameters allow good fits for a range of Σ_m .

In conclusion, we are encouraged by the good agreement between the N -body and Fisher matrix results. The fact that the σ_α from the N -body fits are not much worse than those from the Fisher matrix indicates that our estimator is extracting most of the acoustic information.

7. EFFECTS OF VARIATIONS IN THE TEMPLATE COSMOLOGY

When the true acoustic scale is known, the observations of the BAO allow us to measure the cosmological distance scale, in particular the angular diameter distance $D_A(z)$ and the Hubble parameter $H(z)$. The true acoustic scale is determined from measurements of the matter and baryon density, e.g., from CMB anisotropy data. In this paper, we do not marginalize over uncertainties in the cosmological densities but instead use a fixed fiducial template. Using a fiducial template power spectrum assumes that a true acoustic scale as well as the shape of the linear power spectrum is known a priori.

Here we investigate how the results depend on small deviations in the template power spectrum. We consider variations in $\Omega_m h^2$, $\Omega_b h^2$, and the spectral tilt n of 2%, chosen to be somewhat larger than the expected uncertainties from Planck CMB anisotropy data. When one uses a different cosmological template compared to the true simulation input, one of course measures a shift in α . However, this shift in α is very close to that predicted by the ratio of the sound horizons in the two cosmologies, where the sound horizon r_s is given by equation (6) in Eisenstein & Hu (1998). We find that α/r_s is recovered to no worse than $\pm 0.02\%$ within the above cosmological variations, as shown in Table 6.

This implies that the measured acoustic scale is consistently determined, independent of reasonable variations in the template cosmology. Applying this standard ruler to cosmological distance inferences, one will consistently measure $D_A(z)/r_s$ and $H(z)r_s$ despite variations in the template used. Of course, when one tests a given cosmology against a suite of cosmological measurements, one must account for the change in r_s in using the BAO constraints, just as one must self-consistently alter any other predictions for cosmological observables.

8. CONCLUSIONS

Baryon acoustic oscillations in large-scale structure can serve as an excellent standard ruler to probe the acceleration history of the Universe. Such a standard ruler method is based on the premise that the characteristic scale of the feature, the sound horizon scale, is well measured from CMB and remains fixed throughout the evolution of the Universe.

In this paper, we have measured the shift in the acoustic scale with high signal-to-noise ratio using $320h^{-3} \text{ Gpc}^3$ volume of the PM simulations. We allow a large number of parameters in our fitting formula so that the standard ruler method is dominated by the BAO.

We find nonlinear growth decreases the measured acoustic scale by less than 1%: we find shifts of 0.20% at $z = 1.5$, 0.26% at $z = 1$, 0.33% at $z = 0.7$, and 0.45% at $z = 0.3$, all determined at 5 to 8σ . In detail, we find the redshift dependence of $\alpha - 1$ scales as $D^{1.66^{+0.26}_{-0.22}}$, where D is the linear growth function. The perturbation theory prediction of a D^2 scaling is consistent at 1.3σ . We consider different fitting formula, polynomial orders, and resampling methods and find highly consistent results between various choices.

Our detection of a sub-percent-level shift in the acoustic scale agrees with the analytic node-by-node predictions of nonlinear mode-coupling shift by Crocce & Scoccimarro (2008) within the same order of magnitude. The agreement is better when we compare our results with the shifts they predict assuming a global fit.

Redshift distortions increase the shift by $\sim 25\%$ relative to real space. Using $216h^{-3} \text{ Gpc}^3$ of simulations, we detect a shift of 0.25% at $z = 1.5$, 0.33% at $z = 1$, 0.41% at $z = 0.7$, 0.54% at $z = 0.3$ at the level of 5 to 6σ .

Although our results confirm the previous analytic prediction that nonlinear growth and redshift distortions induce a small mode-coupling shift on the acoustic scale, we find that the shift can be reduced to less than 0.1% by undoing the nonlinear growth using a simple reconstruc-

tion scheme (Eisenstein et al. 2007), even in the presence of non-negligible shot noise.

We compare our results from N -body simulations with the analytic Fisher matrix error forecasts based on Seo & Eisenstein (2007). We find the standard ruler method from the simulations and Fisher formalism forecasts are in agreement within a modest level of sample variance. In detail, we find that σ_α from the simulations is systematically better, by no more than 27%, than the Fisher matrix calculations. While this trend could have an underlying physical cause, it is consistent with sample variance, correlated between redshifts, from our limited number of simulations.

We show that small variations in the template power spectrum around the true fiducial cosmology do not affect our results of α/r_s . Therefore, the cosmological distance ratios $D_A(z)/r_s$ and $H(z)r_s$ inferred from the measurements of the acoustic scale are robust to reasonable errors in the template cosmology.

We argue that it is correct and appropriate to use the linear theory power spectra as a template for extracting the acoustic scale. The acoustic oscillations are not a perfect harmonic sequence nor perfectly exponentially damped. For example, because of Silk damping (Silk 1968), small-scale perturbations in the baryons decouple from the CMB earlier than large-scale perturbations, implying that the sound horizon is not a single quantity. However, the correct waveform is computed in great detail in the Boltzmann codes. Using an approximate waveform will simply risk a loss of precision and accuracy. The exact relation of the acoustic signature and acoustic scale in the CMB to that in the low-redshift large-scale structure depends upon the details of recombination, but this is exquisitely constrained by CMB observations. Once one has accepted the assumptions in interpreting the CMB anisotropies to measure the densities needed to set the sound horizon, it is straight-forward to use the predicted waveform for the low-redshift power spectrum.

Finally, we emphasize that the nonlinear shifts on the acoustic scale are predictable numerically, as shown here for each estimator. With such a prediction, the shifts can be properly modeled and therefore can be removed in the standard ruler analysis of actual clustering data, even without reconstruction; the results can be cross-checked for consistency with the results after reconstruction, when available.

We have successfully computed the effects of nonlinear growth and redshift distortions on the acoustic scale using a large volume of simulated Universe. The galaxy power spectrum is expected to exhibit somewhat larger shifts than the matter power spectrum, as galaxies would sample more nonlinear regions. We will investigate this in a separate paper (Siegel et al., in preparation). Encouraged by the successful reduction of shift by a reconstruction technique applied to the mass distribution with a nonzero shot noise, we will also investigate the use of reconstruction of BAO in the galaxy power spectrum in future work.

We thank Martin Crocce for useful conversations. H.-J.S. is supported by the DOE at Fermilab. E.R.S., D.J.E., and M.W. were supported by NASA grant

NNX07AH11G. E.R.S. and D.J.E. were supported by NASA grant NNX07AC51G and NSF AST-0707725.

The simulations reported here used resources at the National Energy Research Supercomputing Center.

REFERENCES

- Amendola, L., Quercellini, C., & Giallongo, E. 2005, *MNRAS*, 357, 429
- Angulo, R., Baugh, C. M., Frenk, C. S., Bower, R. G., Jenkins, A., & Morris, S. L. 2005, *MNRAS*, 362, L25
- Angulo, R. E., Baugh, C. M., Frenk, C. S., & Lacey, C. G. 2008, *MNRAS*, 383, 755
- Bennett, C. L., et al. 2003, *ApJS*, 148, 1
- Benoît, A. et al. 2003, *A&A*, 399, L19
- de Bernardis, P., et al., 2000, *Nature*, 404, 955
- Bharadwaj, S. 1996, *ApJ*, 472, 1
- Bharadwaj, S. 1996, *ApJ*, 460, 28
- Blake, C., & Glazebrook, K. 2003, *ApJ*, 594, 665
- Blake, C., & Bridle, S. 2005, *MNRAS*, 363, 1329
- Blake, C., Parkinson, D., Bassett, B., Glazebrook, K., Kunz, M., & Nichol, R. C. 2006, *MNRAS*, 365, 255
- Blake, C., Collister, A., Bridle, S., & Lahav, O. 2007, *MNRAS*, 374, 1527
- Bond, J.R. & Efstathiou, G. 1984, *ApJ*, 285, L45
- Cole, S., et al. 2005, *MNRAS*, 362, 505
- Cooray, A. 2004, *MNRAS*, 348, 250
- Crocce, M., & Scoccimarro, R. 2006, *Phys. Rev. D*, 73, 063520
- Crocce, M., & Scoccimarro, R. 2008, *Phys. Rev. D*, 77, 023533
- de Lapparent, V., Geller, M. J., & Huchra, J. P. 1986, *ApJ*, 302, L1
- Dolney, D., Jain, B., & Takada, M. 2006, *MNRAS*, 366, 884
- Eisenstein, D. J., & Hu, W. 1998, *ApJ*, 496, 605
- Eisenstein, D. J., Hu, W., & Tegmark, M. 1998, *ApJ*, 504, L57
- Eisenstein, D.J., 2003, in *ASP Conference Series*, volume 280, *Next Generation Wide Field Multi-Object Spectroscopy*, ed. M.J.I. Brown & A. Dey (ASP: San Francisco) pp. 35-43; astro-ph/0301623
- Eisenstein, D. J., et al. 2005, *ApJ*, 633, 560
- Eisenstein, D. J., Seo, H.-J., Sirko, E., & Spergel, D. N. 2007, *ApJ*, 664, 675
- Eisenstein, D. J., Seo, H.-J., & White, M. 2007, *ApJ*, 664, 660
- Estrada, J., Sefusatti, E., & Frieman, J. A. 2008, *ArXiv e-prints*, 801, arXiv:0801.3485
- Glazebrook, K., & Blake, C. 2005, *ApJ*, 631, 1
- Guzik, J., Bernstein, G., & Smith, R. E. 2007, *MNRAS*, 375, 1329
- Halverson, N. W. et al. 2002, *ApJ*, 568, 38
- Hamilton, A.J.S., 1998, "The Evolving Universe", ed. D. Hamilton (Kluwer: Dordrecht), p. 185; astro-ph/9708102
- Hanany, S., et al., 2000, *ApJ*, 545, L5
- Hinshaw, G., et al. 2007, *ApJS*, 170, 288
- Hinshaw, G., et al. 2008, *ArXiv e-prints*, 803, arXiv:0803.0732
- Holtzman, J. A. 1989, *ApJS*, 71, 1
- Hu, W., & Sugiyama, N. 1996, *ApJ*, 471, 542
- Hu, W., & Haiman, Z. 2003, *Phys. Rev. D*, 68, 063004
- Hu, W., & White, M. 1996, *ApJ*, 471, 30
- Huff, E., Schulz, A. E., White, M., Schlegel, D. J., & Warren, M. S. 2007, *Astroparticle Physics*, 26, 351
- Hütsi, G. 2006, *A&A*, 449, 891
- Jain, B., & Bertschinger, E. 1994, *ApJ*, 431, 495
- Jeong, D., & Komatsu, E. 2006, *ApJ*, 651, 619
- Juszkiewicz, R. 1981, *MNRAS*, 197, 931
- Kaiser, N. 1987, *MNRAS*, 227, 1
- Lee, A. T., et al. 2001, *ApJ*, 561, L1
- Linder, E. V. 2003, *Phys. Rev. D*, 68, 083504
- Ma, Z. 2007, *ApJ*, 665, 887
- Makino, N., Sasaki, M., & Suto, Y. 1992, *Phys. Rev. D*, 46, 585
- Matarrese, S., & Pietroni, M. 2007, *ArXiv Astrophysics e-prints*, arXiv:astro-ph/0703563
- Matsubara, T. 2004, *ApJ*, 615, 573
- Matsubara, T. 2008, *Phys. Rev. D*, 77, 063530
- Meiksin, A., White, M., & Peacock, J. A. 1999, *MNRAS*, 304, 851
- Meiksin, A., & White, M. 1999, *MNRAS*, 308, 1179
- Miller, A.D., Caldwell, R., Devlin, M.J., Dorwart, W.B., Herbig, T., Nolta, M.R., Page, L.A., Puchalla, J., Torbet, E., & Tran, H.T., 1999, *ApJ*, 524, L1
- Netterfield, C. B., et al. 2002, *ApJ*, 571, 604
- Nishimichi, T., et al. 2007, *PASJ*, 59, 1049
- Okumura, T., Matsubara, T., Eisenstein, D. J., Kayo, I., Hikage, C., Szalay, A. S., & Schneider, D. P. 2008, *ApJ*, 676, 889
- Padmanabhan, N., et al. 2007, *MNRAS*, 378, 852
- Padmanabhan, N., & White, M. 2008, *ArXiv e-prints*, 804, arXiv:0804.0799
- Papai, P., & Szapudi, I. 2008, *ArXiv e-prints*, 802, arXiv:0802.2940
- Pearson, T. J., et al. 2003, *ApJ*, 591, 556
- Peebles, P. J. E. & Yu, J. T. 1970, *ApJ*, 162, 815
- Percival, W. J., et al. 2007, *ApJ*, 657, 51
- Percival, W. J., Cole, S., Eisenstein, D. J., Nichol, R. C., Peacock, J. A., Pope, A. C., & Szalay, A. S. 2007, *MNRAS*, 381, 1053
- Perlmutter, S. et al. 1999, *ApJ*, 517, 565
- Riess, A. G. et al. 1998, *AJ*, 116, 1009
- Sanchez, A. G., Baugh, C. M., & Angulo, R. 2008, *MNRAS*, submitted (arXiv:0804.0233)
- Scoccimarro, R., Zaldarriaga, M., & Hui, L. 1999, *ApJ*, 527, 1
- Scoccimarro, R. 2004, *Phys. Rev. D*, 70, 083007
- Seljak, U., Sugiyama, N., White, M., & Zaldarriaga, M. 2003, *Phys. Rev. D*, 68, 083507
- Seljak, U., & Zaldarriaga, M., 1996, *ApJ*, 469, 437
- Seo, H.-J., & Eisenstein, D. J. 2003, *ApJ*, 598, 720
- Seo, H.-J., & Eisenstein, D. J. 2005, *ApJ*, 633, 575
- Seo, H.-J., & Eisenstein, D. J. 2007, *ApJ*, 665, 14
- Silk, J. 1968, *ApJ*, 151, 459
- Smith, R. E., Scoccimarro, R., & Sheth, R. K. 2007, *Phys. Rev. D*, 75, 063512
- Smith, R. E., Scoccimarro, R., & Sheth, R. K. 2008, *Phys. Rev. D*, 77, 043525
- Springel, V., et al. 2005, *Nature*, 435, 629
- Sunyaev, R. A., & Zeldovich, Y. B. 1970, *Ap&SS*, 7, 3
- Takahashi, R., et al. 2008, *ArXiv e-prints*, 802, arXiv:0802.1808
- Tegmark, M., et al. 2006, *Phys. Rev. D*, 74, 123507
- Vishniac, E. T. 1983, *MNRAS*, 203, 345
- Wagner, C., Müller, V., & Steinmetz, M. 2007, arXiv:0705.0354
- White, M., & Scott, D. 1996, *ApJ*, 459, 415
- White, M. 2005, *Astroparticle Physics*, 24, 334
- Zhan, H., & Knox, L. 2006, *ApJ*, 644, 663
- Zel'dovich, Y.A., 1970, *A&A*, 5, 84

TABLE 1
THE MEAN AND THE ERROR OF α IN REAL SPACE

z	Model	Σ_m	$\alpha - 1(\%)$	$\sigma_\alpha(\%)$	χ^2/DOF
0.3	Poly7	7.6	0.45	0.055	1.09
0.3	Pade	7.6	0.45	0.057	1.00
0.3	Poly3	7.6	0.43	0.056	1.24
0.7	Poly7	6.3	0.33	0.046	1.10
0.7	Pade	6.3	0.33	0.046	0.97
1.0	Poly7	5.5	0.27	0.041	1.13
1.0	Pade	5.5	0.26	0.042	0.99
1.5	Poly7	4.5	0.20	0.037	1.17
1.5	Pade	4.5	0.20	0.037	1.04
0.3	Pade	6.0	0.45	0.057	0.98
0.3	Pade	7.0	0.45	0.057	0.99
0.3	Pade	10.0	0.45	0.057	1.03

NOTE. — Fitting range: $0.02h \text{ Mpc}^{-1} \leq k \leq 0.35h \text{ Mpc}^{-1}$ (a total of 70 data points). Reduced χ^2 , χ^2/DOF , where “DOF” is the number of degrees of freedom, is calculated from the best fit to the averaged power spectra over $320h^{-3} \text{ Gpc}^3$.

TABLE 2
THE MEAN AND THE ERROR OF α IN REDSHIFT SPACE.

z	Model	Σ_m	$\alpha - 1(\%)$	$\sigma_\alpha(\%)$	χ^2/DOF
0.3	Poly-Exp-Out	9.0	0.54	0.070 (0.085)	1.26
	Poly-Exp-In	9.0	0.55	0.070 (0.086)	1.25
	Poly7	9.0	0.54	0.068 (0.083)	1.24
	Poly-Rat-In	9.0	0.50	0.084 (0.103)	1.46
	Poly-Rat-Out	9.0	0.53	0.069 (0.084)	1.23
	Pade-Rat-In	9.0	0.55	0.077 (0.093)	1.28
0.7	Poly-Exp-Out	8.0	0.41	0.057 (0.069)	1.12
1.0	Poly-Exp-Out	7.0	0.33	0.049 (0.060)	1.10
1.5	Poly-Exp-Out	6.0	0.25	0.041 (0.050)	1.11
0.3	Poly-Exp-Out	8.0	0.54	0.071 (0.086)	1.268
0.3	Poly-Exp-Out	9.0	0.54	0.070 (0.085)	1.256
0.3	Poly-Exp-Out	10.0	0.54	0.070 (0.085)	1.259
0.3	Poly-Exp-Out	11.0	0.57	0.070 (0.085)	1.413

NOTE. — Fitting range: $0.02h \text{ Mpc}^{-1} \leq k \leq 0.35h \text{ Mpc}^{-1}$. Values of σ_α from the N -body (the fifth column) are the errors for 40 simulations ($320h^{-3} \text{ Gpc}^3$) rescaled from the errors for 27 simulations ($216h^{-3} \text{ Gpc}^3$). The actual errors for 27 simulations are listed within the parentheses. Reduced χ^2 is calculated from the best fit to the averaged power spectra over $216h^{-3} \text{ Gpc}^3$.

TABLE 3
THE EFFECT OF DENSITY-FIELD RECONSTRUCTION IN REAL SPACE.

z	Model	Before Reconstruction				After Reconstruction			
		Σ_m	$\alpha - 1(\%)$	$\sigma_\alpha(\%)$	χ^2/DOF	Σ_m	$\alpha - 1(\%)$	$\sigma_\alpha(\%)$	χ^2/DOF
0.3	Poly7	7.6	0.40	0.071	1.09	3.0	0.07	0.044	1.15
0.7	Poly7	6.3	0.27	0.062	1.07	2.0	0.03	0.049	1.19
1.0	Poly7	5.5	0.22	0.075	1.00	2.0	0.00	0.052	1.13
1.5	Poly7	4.5	0.19	0.079	0.99	2.0	0.03	0.080	1.04

NOTE. — Fitting range: $0.02h \text{ Mpc}^{-1} \leq k \leq 0.5h \text{ Mpc}^{-1}$ (a total of 481 data points). We use the 1% sample.

TABLE 4
THE EFFECT OF DENSITY-FIELD RECONSTRUCTION IN REDSHIFT SPACE

z	Model	Before Reconstruction				After Reconstruction			
		Σ_m	$\alpha - 1(\%)$	$\sigma_\alpha(\%)$	χ^2/DOF	Σ_m	$\alpha - 1(\%)$	$\sigma_\alpha(\%)$	χ^2/DOF
0.3	Poly-Exp-Out	9.0	0.48	0.079	1.31	4.0	0.07	0.046	1.20
0.7	Poly-Exp-Out	8.0	0.30	0.081	1.14	4.0	0.03	0.047	1.21
1.0	Poly-Exp-Out	7.0	0.31	0.093	1.19	3.0	0.01	0.056	1.28
1.5	Poly-Exp-Out	6.0	0.27	0.079	1.08	3.0	0.04	0.070	1.19

NOTE. — Fitting range: $0.02h \text{ Mpc}^{-1} \leq k \leq 0.5h \text{ Mpc}^{-1}$. We use the 1% sample.

TABLE 5
FISHER MATRIX ESTIMATES IN COMPARISON TO SIMULATION RESULTS

	N-body data				Fisher matrix		
	z	Sample	Σ_m	$\sigma_\alpha(\%)$	Σ_{nl}	$nP_{0.2}$	σ_α
Real space	0.3	100%	7.6	0.055	7.6	100	0.068
	0.7	100%	6.3	0.046	6.3	100	0.054
	1.0	100%	5.5	0.041	5.5	100	0.047
	1.5	100%	4.5	0.037	4.5	100	0.039
	0.3	1%	7.6	0.071	7.6	2.36	0.084
	0.7	1%	6.3	0.062	6.3	1.47	0.076
	1.0	1%	5.5	0.075	5.5	1.10	0.075
	1.5	1%	4.5	0.079	4.5	0.72	0.078
	z	Sample	Σ_m	$\sigma_\alpha(\%)$	Σ_{xy}/Σ_z	$nP_{0.2}(\mu=0)$	σ_α
Redshift space	0.3	100%	9.0	0.070 (0.085)	7.6/12.1	100	0.085
	0.7	100%	9.0	0.058 (0.071)	6.3/11.0	100	0.069
	1.0	100%	7.0	0.049 (0.060)	5.5/10.1	100	0.060
	1.5	100%	6.0	0.041 (0.050)	4.5/8.6	100	0.049
	0.3	1%	9.0	0.079	7.6/12.1	2.36	0.10
	0.7	1%	8.0	0.081	6.3/11.0	1.47	0.089
	1.0	1%	7.0	0.093	5.5/10.1	1.10	0.084
	1.5	1%	6.0	0.079	4.5/8.6	0.72	0.081

NOTE. — Values of Σ_m in the fourth column represents the nonlinear smoothing used for the template $P(k)$ in the χ^2 analysis of the N -body data, and Σ_{nl} and Σ_{xy}/Σ_z in the sixth column are derived from the Zel'dovich approximations and represents the nonlinear degradation of the BAO assumed in the Fisher matrix calculations. For the 100% samples in redshift space, we list both the actual σ_α from the 27 simulations (inside the parentheses) and the rescaled σ_α for 40 simulations.

TABLE 6
THE EFFECT OF A TEMPLATE P_m WITH AN INCORRECT COSMOLOGY

	z	Cosmology Alteration	Ratio of α/r_s
Real space	0.3	1.02 $\Omega_m h^2$	1.0002
	0.3	0.98 $\Omega_m h^2$	0.9998
	0.3	1.02 $\Omega_b h^2$	0.9999
	0.3	$n_s = 0.95$	1.0000
	1.5	1.02 $\Omega_m h^2$	1.0002
Redshift space	0.3	1.02 $\Omega_m h^2$	1.0001
	1.5	1.02 $\Omega_m h^2$	1.0002

NOTE. — The ratio of α/r_s , where r_s is the sound horizon, in the fourth column compares the values of α/r_s from an incorrect cosmology template with the one from the fiducial cosmology. Our fiducial cosmology is $\Omega_m h^2 = 0.1225$, $\Omega_b h^2 = 0.0224$, and $n = 0.97$. Fitting range: $0.02h \text{ Mpc}^{-1} \leq k \leq 0.35h \text{ Mpc}^{-1}$. We use the 100% sample.